Echelle spectrograph at the 2.6 m Shajn telescope

A.F. Lagutin, S.I. Plachinda, D.N. Shakhovskoy, E.M. Nekhay, D.N. Baklanova, P.P. Petrov

Crimean Astrophysical Observatory, Nauchny 298409, Crimea
e-mail: dilyara@craocrimea.ru

ABSTRACT

The paper describes the high-resolution echelle spectrograph ESPL developed for the coude focus of the 2.6 m Shajn reflector of the Crimean Astrophysical Observatory. The spectrograph has been regularly operated since 2013. Efficiency of the spectrograph is estimated from observations of stars.

Key words: astronomy, instruments, observational facilities, spectrometry

1 Introduction

The reflector named after academician G.A. Shajn (ZTSh), put into operation at the Crimean Astrophysical Observatory AS USSR (CrAO) in the early 1960s, was equipped with the classical spectrograph ASP-114 in the coude focus (Vasil'ev, 1976). The spectrograph had three optical cameras with various inverse dispersions, from 1.6 to 12 Å/mm. Spectra were recorded on photoplates. In 1985 ASP-14 was equipped with the CCD camera to record spectra with resolution $R \sim 30000$ at a slit width of 1 arcsec. The small size of the CCD receiver significantly limits the recorded spectrum range. There appeared a necessity to create a new – echelle – spectrograph which enables one to project many spectral orders onto the CCD, and thus to record a significantly larger wavelength range.

The first experience of creating an echelle spectrograph for ZTSh was described by I.M. Kopylov and N.V. Steshenko in 1965 (Kopylov, Steshenko, 1965). The new echelle spectrograph for the coude focus of ZTSh was designed in the late 1990s and made in the early 2000s at CrAO. In 2013, after being equipped with the CCD camera ANDOR with a chip of $2k \times 2k$ and a pixel size of 13.5 mkm, the spectrograph was used for systematic spectral and spectropolarimetric observations. The spectrograph was shortly named ESPL (Echelle Spectrograph by Pronik and Lagutin) after its two main designers. The current paper presents a short description of the optical layout and mechanical construction of the spectrograph, as well as its characteristics derived in the course of stellar observations.

The classical optical layout of the spectrograph for the coude focus of ZTSh was calculated by V.I. Pronik. Optical elements and the beam path in the spectrograph are schematically shown in Fig. 1. The convergence of the light beam in the coude focus is 1:40, therefore the spectrograph has a comparatively large size: at a diameter of the collimated beam of 150 mm the distance from the entrance slit to the collimator is 6 meters.
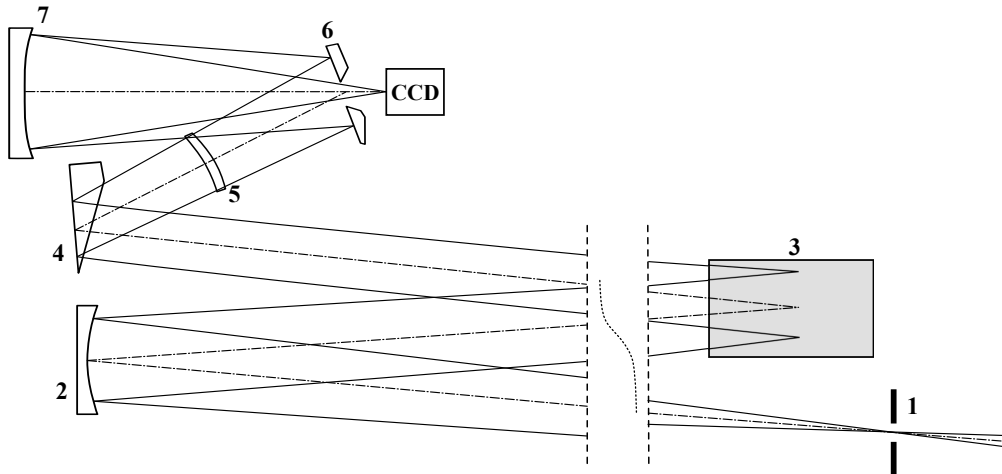
2 Optical layout of the spectrograph

The diameter of the collimator mirror $D_{col} = 160$ mm, the collimator focus $F_{col} = 6020$ mm. The echelle seems to be a replica manufactured at the Vavilov State Optical Institute in 2005. The size of the hatched region is 410×200 mm, the number of lines per millimeter is 37.5, the total number of lines is 15375. The blazing angle is $63°10'$. The distance from the collimator up to the echelle is 4000 mm. The distance between optical elements in the collimator and camera unit is shown in Fig. 2.
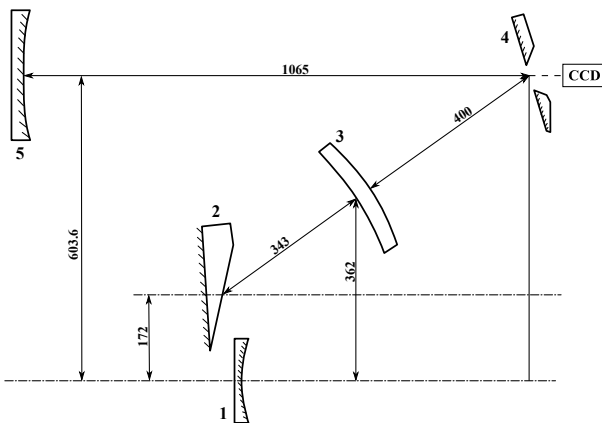
The spectrograph has two changeable cross-dispersing elements: a prisma and a diffraction grid. The prism is made of glass F1. The back side of the prism is aluminized. The light goes through the prism twice, as a result, the prism deflection angle equals 34°. The diffraction grid (replica) was also made at the Vavilov State Optical Institute in 2005. Sizes of the replica hatched region are 200×300 mm, 150 lines per 1 mm, the total number of lines is 30000. The grid provides the predominant light concentration in a region of 4000–12000 Å in the first order. The grid concentrates ~ 70 % of the reflected light at a wavelength of $\lambda 6328$ Å.

After the cross-dispersor light goes through the corrector (meniscus) to the flat mirror and is reflected to the spherical camera mirror. The meniscus is made of glass K8, the curvature radii of the concave and convex surfaces are 445.5 and 466.4 mm, respectively. The diameter of the camera mirror $D_{cam} = 350$ mm, the curvature radius $R_{cam} = 2211$ mm. The camera focal length, given the optical refracting power of the meniscus and the distance between two elements, is 1105.5 mm. From the camera mirror the convergent light goes through the central hole in the flat mirror and is focused on the light receiver (see in what follows). Since in the light beam from ZTSh there is a central blanketing by the secondary mirror, the hole in the flat mirror in the spectrograph camera causes no additional light loss.

The focal length of the ZTSh coude system equals 104204 mm (Vasil'ev, 1976). The modeling of the spectro-

Fig. 1. Optical layout of the spectrograph: 1 – entrance slit, 2 – collimator, 3 – echelle, 4 – cross-dispersor, 5 – corrector, 6 – flat mirror, 7 – camera mirror, 8 – CCD camera

Fig. 2. Optical layout of the collimator unit and camera: 1 – collimator, 2 – cross-dispersing prism, 3 – corrector, 4 – flat mirror, 5 – camera mirror. Distance is expressed in mm

graph optical system in the program ZEMAX yields the value of the equivalent focal length of the telescope+spectrograph system F_e = 18488 mm. The corresponding scale in the spectrograph focal plane is 0.0896 mm/arcsec.

Fig. 3 shows a spectrum image while using the prism for cross-dispersion, and Fig. 4 demonstrates a spectrum image while using the diffraction grid. In the second case the distance between spectral orders is larger; this allows us to set an analyzer of circularly polarized light, so-called 'stokesmeter' (Plachinda, 2005).

Provision is made for introducing a flat mirror in front of the echelle. In this case only prisma (or a grid) serves as a dispersing element. This variant is mostly used during the spectrograph alignment. The spectrograph was initially projected based on the pixel size of the CCD equal to 24 mkm. In this case, at a width of the entrance slit of 11 arcsec (0.505 mm), its projection onto the CCD would be ∼ 3.7 pixels. The camera ANDOR with a chip size of $2k \times 2k$ and a pixel size of 13.5 mkm is currently used as a standard camera. Whereas the projection of an entrance slit of 1 arcsec onto

the CCD is equal to ∼ 6.637 pixels, and the corresponding spectral resolution $R \sim 48026$.

The most number of clear nights in CrAO is in the summer-autumn period when the average image quality is about 2 arcsec, therefore many observation programs with ESPL are performed with an entrance slit of 2 arcsec. In this case the projection of the entrance slit on the CCD is ∼ 13.3 pixels and the spectral resolution $R \sim 24013$. To increase the dynamic range and to decrease noise, there was sometimes applied a binning per 4 pixels along the dispersion, thus ≈ 3.3 bins fall on the entrance slit width.

3 Mechanical part of the spectrograph

The spectrograph has large longitudinal distance between optical elements, which are mainly grouped at the ends of the device. Hence, there are high requirements to stiffness of the mechanical part that ties optical knots. The location of spectrograph's basic knots is schematically shown in Fig. 5.

The spectrograph is located on the concrete foundation that is untied from the telescope foundation and moving part of the telescope. The basement of the device is represented by a concrete bridge of the furrowed section supported on two footings. Concrete is overlaid by steel plates to which spectrograph's optical and mechanical knots are attached. All the optical details are fixed up into the rims or on bearing frames which are capable of small displacements with adjustable mounting screws tightened up after the device alignment.

The spectrograph is mounted horizontally in the isolated room of the eastern part of the telescope tower; this provides minimum (≤ 2 °C) temperature variations during an astronomical night. The telescope light beam is intercepted by a small switching flat mirror near the coude focus and is directed horizontally to the spectrograph's entrance slit.
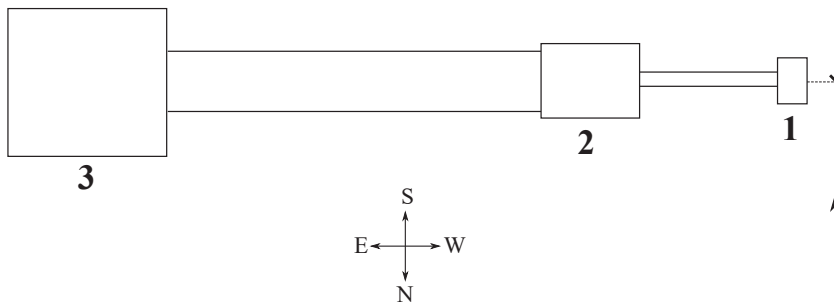
The spectrograph's *entrance slit* has a complex construction with the tangent screw which enables a precise set of the slit width. The front plane of slit sidepieces is reflecting; this allows one to use stellar image edges in the photoelectric guiding device attached to the telescope, in the visual control

Fig. 3. Images of the SU Aur (G2 IVe) spectrum on-screen when using the prism as a cross-dispersor. The red region is at the top. The broad H_α emission line with central absorption is seen at the top left, and the sodium doublet - at the lower right

Fig. 4. An image of the β Aql (G8 IV) spectrum on-screen when using the diffraction grid as a cross-dispersor. The red region is at the bottom. The spectrum is derived with an analyzer of circularly polarized light, therefore each order is divided into two spectra. The strong line is in the lower part of the image – H_α. The sodium doublet is well seen in the top right corner

Fig. 5. Layout of the location of spectrograph's basic knots (top view): 1 – entrance slit unit, 2 – echelle unit, 3 – collimator and camera unit

system, and in other elements of the near-slit part previously described by (Lagutin, 2011).

Echelle is located in the rim equipped with two ball step bearings which vertically fix the echelle rotation axis (echelle lines are vertical). The echelle rotation is carried out with an arcsine mechanism in which the standard tangent screw rotated by the step motor serves as a pusher.
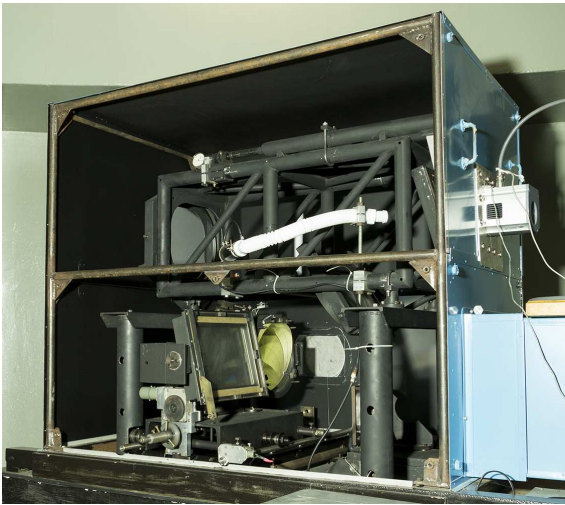
Flat mirror in front of the echelle is mounted in the construction that allows a mirror to be introduced into the light beam by rotating around the horizontal axis, which is perpendicular to the mirror plane.

Cross-dispersing elements – *prism* and *diffraction grid* (grid lines are horizontal) – are fixed nearby, on the rigid elbow-type detail capable of tilting around the horizontal axis on two balls by means of a mechanism with the pusher, which is analogous to the echelle mechanism. All the installation is fixed on a bogie driven by the lead screw along guide ways in the transverse direction to introduce into the beam of the prism or the grid. Rotations of the echelle, prism and

grid prescribed remotely by means of step motors allow the required spectrum regions to be introduced into the CCD frame.

CCD camera was hanged on the focus frame capable of moving along the optical axis with a rigid fixing of the position after focusing; the standard point indicator was mounted to measure the distance of movement. Optical elements of the camera are tied by a rigid support welded from tubes and serving as a base for the focus frame.

All the spectrograph construction is covered into the light-protective wrapper that consists of two – eastern and western – containers and a tube of the box-like section that connects them. The wrapper elements are put together from aluminum sheets on steel carcasses. On the way of light beams in some places of the spectrograph there are elements for limiting beams – diaphragms that prevent from possible parasitic illumination. All inner surfaces of the wrapper, as well as light-proof rooms in which the spectrograph is positioned, are painted in black.

Fig. 6. Collimator and camera unit

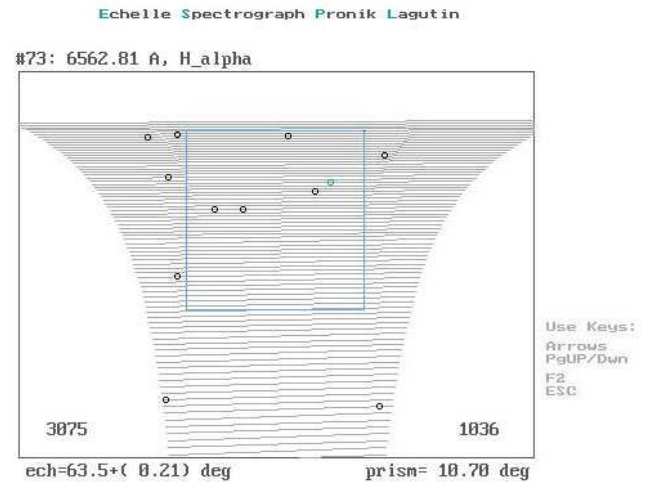The general view of the collimator and camera unit is presented in Fig. 6.

4 Control and registration system

Spectrograph elements are controlled with a controller designed at CrAO. The program written specially for the data exchange with this controller, using the computer port RS-232, allows one to control switching on the lamps of the comparison spectrum and flat field, and three step motors. Two motors regulate the echelle's horizontal rotation angle and the vertical inclination angle of the cross-dispersor. Backlash-free drives of these optical elements are implemented with micrometer screws pushing the spring-loaded rim of the optical element. The third step motor is intended for introducing into the light beam in front of the flat mirror slit. When the mirror is disable, the object image falls on the slit, when it is introduced – the image of lamps does. The mirror is mounted directly on the step motor axis.

The user interface of the program allows a real-time control of the state of spectrograph's movable optical components. It is also possible to remember and restore the position of the prism and grid for various spectral regions. The position of optical elements is controlled by counting steps of the corresponding motor with saving data on the disk drive.

As a detector we use the CCD camera Andor iKon-L 936 with back-illuminated E2V CCD42-40 with 2048×2048 pixels of 13.5 mkm in size, the readout noise is 3 electrons at a digitization frequency of 50 kHz, 7 electrons at a frequency of 1 MHz. The CCD cooling is thermoelectrical, the air cooling mode is usually used, which provides a temperature regulation of $-60\,°C$. A temperature drop of up to $-100\,°C$ is possible by the water cooling system. To operate the exposition, the built-in shutter of the CCD camera is used. To obtain images, the Andor Solis software is used. Viewing and guiding of the object on the spectrograph entrance slit is performed with the camera Meade DSI.

Currently, when using the CCD matrices of the 27.5×27.5 mm format, spectral orders in the CCD frame are not intersected on wavelengths, therefore while planning observations, one previously chooses such rotation angles of the
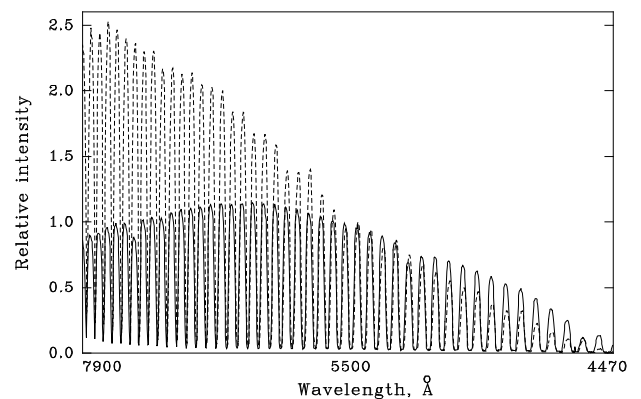

Fig. 7. Diagram showing the location of spectral orders in the spectrograph's focal plane. The red region is at the top. The CCD frame is denoted by a rectangle. Positions of the given spectral lines are marked by circles. Numbers in the lower part of the figure – rotation angles of the echelle and prism
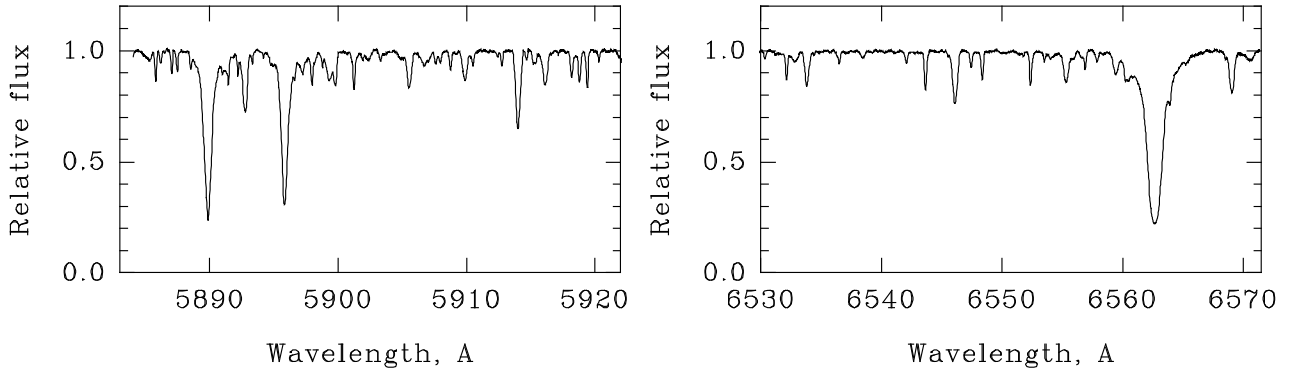
echelle and cross-dispersing element at which the CCD format covers the required spectrum regions. For this aim the program was written that models the image of spectral orders in the focal plane where in the interactive mode, setting up the rotation angles, one may bring up the given spectral lines in the CCD frame. Fig. 7 shows the image on-screen while working with this program in the case of using the prism. In the CCD frame there are CaII 8542 Å (at the top), H_α lines, and the DNa I doublet.
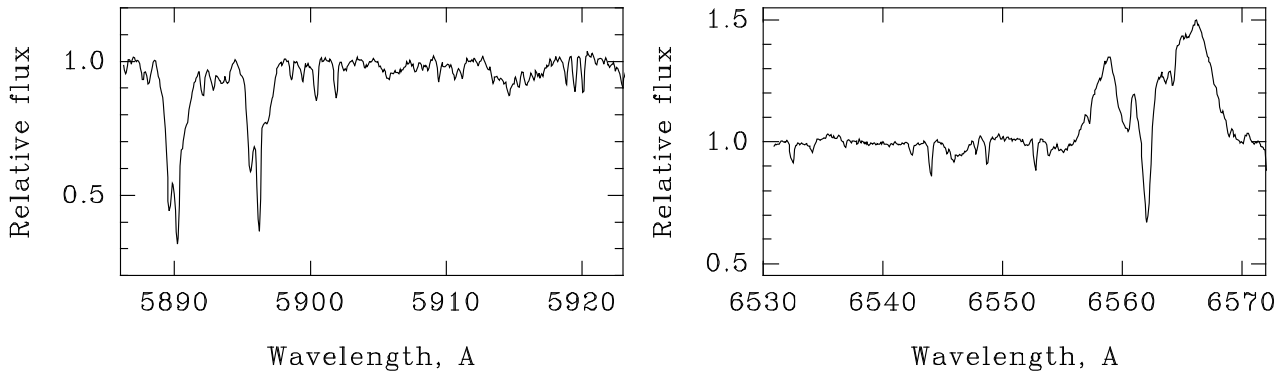
5 Spectrograph's effectiveness

The relative intensity of various spectral orders depends on spectral sensitivity of the CCD matrix and stellar spectral type. Fig. 8 shows photometric sections across spectral or-

Fig. 8. Photometric sections of spectral orders (across dispersion, in the center of the order) of stars of similar magnitude *V*, but different spectral types: solid line – the O7 V star, dotted line – the K0 V star

Fig. 9. Fragments of the η Boo spectrum, G0 IV (spectral orders 81 and 73) derived with an entrance slit of 1 arcsec. Spectral resolution $R = 48000$

Fig. 10. Fragments of the SU Aur spectrum, G2 IVe (spectral orders 81 and 73) derived with an entrance slit of 2 arcsec. Spectral resolution $R = 24000$

ders during observations of early- and late-type stars. Fig. 9 and 10 show examples of stellar spectra.
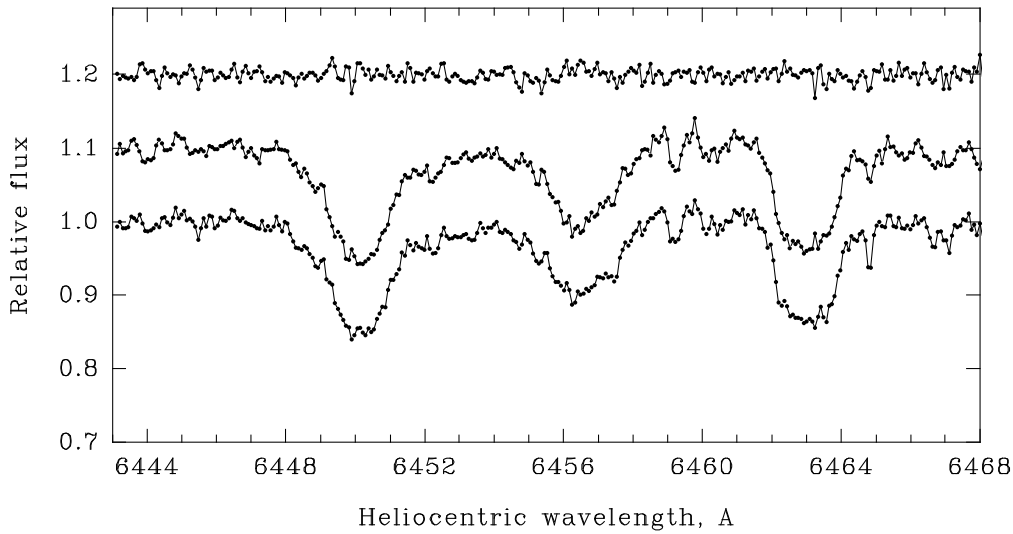
The accuracy of light-of-sight velocity measurements depends on spectral resolution and stability of the element position of the spectrograph's optical system. The spectral resolution element determined as a half-width (FWHM) of the weak atmospheric water lines in the red spectrum region at an entrance slit of 2 arcsec equals ≈ 12 km/s; this corresponds to the calculated spectral resolution. The wavelength scale is determined from the comparison spectrum of lamp Th-Ar. In our case, when using the CCD matrix of the 27.5×27.5 mm format, spectral orders are not intersected on wavelengths, therefore the wavelength scale is defined separately for each order, and the accuracy of this determination is limited by the small number of reference lines in the comparison spectrum of Th-Ar. From measurements of ten spectra of the φ Tau star obtained at different nights in October-November 2018 with a wide slit of 2 arcsec, the root-mean-square deviation of the stellar light-of-sight velocity is ± 0.5 km/s. In the red spectrum region this corresponds to $\sim 1/20$ of the entrance slit width. When using a narrower entrance slit of 11 arcsec, the root-mean-square deviation is twice less. More accurate line-of-sight measurements need the applying of an iodine cell (Perdelwitz, Huke, 2018).

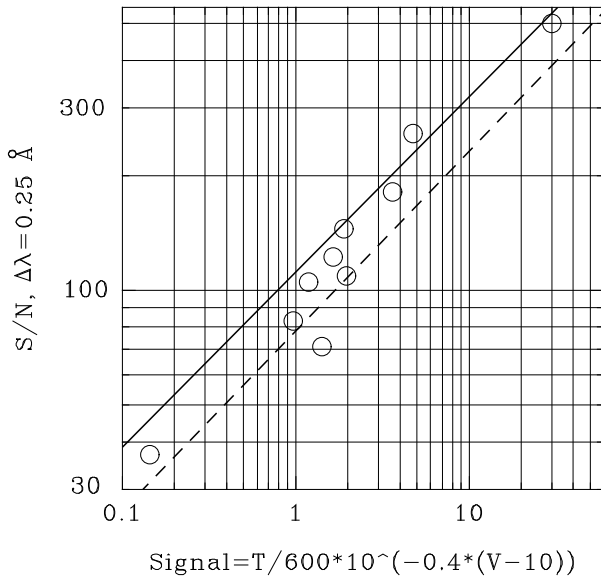The spectrograph's effectiveness can be estimated based on the signal-to-noise ratio (S/N) in stellar spectra depending on the star brightness and exposure duration. For the illustration purposes, Fig. 11 shows fragments of the RY Tau spectra taken on October 11–12, 2018 when the image quality was about 1 arcsec. This is a G2 IV-type star, its brightness at the time of our observations, based on the AAVSO data, is $V = 9^m.40$. Spectra were derived with an entrance slit of 2 arcsec, namely the light losses on the entrance slit were negligibly small. The star was observed at a zenith distance of $\approx 20°$. Several consecutive 30-minute exposures allow us to estimate the signal-to-noise ratio. For the analysis we have chosen the spectral order in the red region.

After the standard image processing routine a ratio of two spectra was calculated, the so called noise track. A noise level of the noise track by $\sqrt{2}$ times exceeds the noise of a single spectrum. The binning routine over four pixels was applied for this particular exposure time. In Figure 11 each point represents data for one bin. A spectral resolution element (~ 0.27 Å) covers approximately 3.3 bins. In the noise track, the signal-to-noise ratio is approximately $S/N = 110$ per bin, which corresponds to $S/N = 110 \times \sqrt{2} \times \sqrt{3.3} \approx 282$ per spectral resolution element for a single spectrum.

Fig. 12 shows the diagram that allows one to determine the expected S/N ratio per resolution element in the red spectrum region depending on the stellar brightness (given the air mass) and the exposure duration at an entrance slit of 2 arcsec. Circles – data obtained on stellar spectra from

Fig. 11. Region of the RY Tau spectrum ($V = 9^m.4$). Bottom curves – two 30-minute exposures derived at the night with good image quality. Top curve – a hash obtained dividing one spectrum into another. Spectra are shifted on the intensity scale

Fig. 12. Signal-to-noise ratio per spectral resolution element ($R = 24000$) depending on the exposure T (sec) and magnitude V. The signal = 1 corresponds to the 10-minute stellar exposure $V = 10^m$

vice is effective enough to resolve many astrophysical tasks. Results of the studies carried out with this spectrograph can be found in publications by (Butkovskaya et al., 2017; Butkovskaya et al., 2018; Pogodin et al., 2018; Petrov et al., 2019; Butkovskaya, Plachinda, 2018; Kozlova et al., 2017; Babina et al., 2016; Potravnov et al., 2017). The spectrograph's resolving power is not fully employed at the typical for CrAO quality of images. The effectiveness of the device may be increased by using a more wide-format CCD.

References

Vasil'ev A.S., 1976. Izv. Krymsk. Astrofiz. Observ., vol. 55, p. 224. (In Russ.)

Kozlova O.V. et al., 2017. Astrofizika, vol. 60, no. 1, p. 41. (In Russ.)

Kopylov I.M., Steshenko N.V., 1965. Izv. Krymsk. Astrofiz. Observ., vol. 33, p. 308. (In Russ.)

Lagutin A.F., 2011. Izv. Krymsk. Astrofiz. Observ., vol. 107, no. 1, p. 183. (In Russ.)

Pogodin M.A. et al., 2018. Astrofizika, vol. 61, p. 15. (In Russ)

Babina E.V. et al.,2016. Astron. Lett., vol. 42, p. 193.

Butkovskaya V.V. et al., 2017. Astron. Nachr., vol. 338, p. 896.

Butkovskaya V.V., Plachinda S.I., 2018. Contr. of the Astron. Obs. Skalnaté Pleso, vol. 48, p. 275.

Butkovskaya V.V. et al., 2018. Contr. of the Astron. Obs. Skalnaté Pleso, vol. 48, p. 273.

Perdelwitz V., Huke, P., 2018. Mon. Not. Roy. Astron. Soc., vol. 479, p. 768.

Petrov P.P. et al., 2019. Mon. Not. Roy. Astron. Soc., vol. 483, p. 132.

Plachinda S.I., 2005. Astrophysics, vol. 48, no. 1, p. 9.

Potravnov I. S. et al., 2017. Astron. Astrophys., vol. 599, p. A60.

5^m to 10^m. The solid line indicates the ratio in the absence of light losses on the entrance slit. The dotted line shows the same ratio at the 50 % light losses. The lines inclination corresponds to the dependence determined by the quantum statistics: $S/N \sim \sqrt{N}$. Data were acquired for the G – K-type stars.

6 Conclusions

The application of the spectrograph ESPL in regular stellar observations throughout several years has shown that the de-